Mixed Sn-Ge Perovskite for Enhanced Perovskite Solar Cell Performance in Air

Mixed Sn-Ge Perovskite for Enhanced Perovskite Solar Cell Performance in Air

Nozomi Ito[a], Muhammad Akmal Kamarudin[a], Daisuke Hirotani[a], Yaohong Zhang[b], Qing Shen[b], Yuhei Ogomi[a], Satoshi Iikubo[a], Takashi Minemoto[c], Kenji Yoshino[d], Shuzi Hayase[a*]*

[a]Graduate School of Life Science and Systems Engineering, Kyushu Institute of Technology, 2-4 Hibikino, Wakamatsu-ku, Kitakyushu-shi, Fukuoka-ken, 808-0196 Japan

[b]Faculty of Informatics and Engineering, The University of Electro-Communications, 1-5-1 Chofugaoka, Chofu, Tokyo, 182-8585 Japan

[c]Department of Electrical and Electronic Engineering, Faculty of Science and Engineering, Ritsumeikan University, 1-1-1, Nojihigashi, Kusatsu, Shiga, 525-8577 Japan

[d]Department of Electrical and Electronic Engineering, Miyazaki University, 1-1 Gakuen Kibanadai Nishi, Miyazaki, 889-2192 Japan

ABSTRACT: Lead-based solar cells have gained ground in recent years, showing efficiency as high as 20 % which is on par with silicon solar cells. However, the toxicity of lead makes it non-ideal candidate in solar cells. Alternatively, tin-based perovskites have been proposed due to their non-toxic nature and abundance in nature. Unfortunately, these solar cells suffer from low efficiency and stability. Here, we propose a new type of perovskite material based on mixed tin and germanium. The material showed a band gap around 1.4 – 1.5 eV as measured from photoacoustic spectroscopy, which is ideal from the perspective of solar cells. In a solar cell device with inverted planar structure, pure tin perovskite solar cell showed a moderate efficiency of 3.31 %. With 5 % doping of germanium into the perovskite, the efficiency improved up to 4.48 % (6.90 % after 72 hours) when measured in air without encapsulation.

TOC Graphic
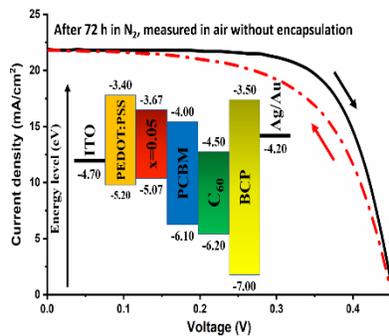
Perovskite-based solar cells were first introduced by Miyasaka *et al*. in 2009 and since then lead-based perovskite solar cells have revolutionized the field of thin-film solar cells showing certified efficiency as high as 21 %[1,2]. The high efficiency of perovskite solar cells come from the high diffusion length of electrons and an ideal band gap of around 1.5 eV which is close to the 1.34 eV limit placed by the Shockley-Queisser limit[3,4]. The diffusion length of lead-based perovskite material has been reported as high as 175 µm for a single crystal material[5]. In addition, the low trap density in lead-based perovskite also contribute to the high performance of the solar cell device[6]. Despite the high-efficiency of these lead-based perovskite solar cells, the problem associated from the toxic nature of lead has open a new research direction which focuses on lead-free perovskite materials[7,8].

As an alternative, Sn has been proposed to replace lead because of its low bandgap of around 1.10 eV in the case of $MASnI_3$. Additionally, Sn is abundant in nature and does not pose a health risk either to human being or to nature. When mixed with Pb, the perovskite showed improved light harvesting energy near the infra-red region which could be exploited further to improve the efficiency of the solar cells[9]. The highest efficiency obtained with Sn only perovskite was 9 % which was based on 2D and 3D mixture of $FASnI_3$[10]. However, Sn-based perovskites are known to have low stability in air in which Sn readily oxidizes from +2 to +4 upon exposure to air leaving oxygen vacancies which act as traps[11–13].

Another alternative candidate to replace lead is Ge. Stoumpos *et al*. first suggested the prospect of Ge-based perovskite material by preparing series of Ge-based perovskites using different cations[14]. The group studied the optical and electrical properties of the perovskites and found that the E_g ranging from 1.60 to 3.80 eV. However, no data was given on the solar cell performance of the materials. The use of Ge-based perovskite in solar cell was first realized by

Krishnamoorthy *et al.*[15]. The measured solar cell performance was notably low, 0.11 % for

CsGeI$_3$ and 0.20 % for MAGeI$_3$. A theoretical study exploring hybrid Sn and Ge perovskite

showed that it is possible to prepare a stable Sn-Ge perovskite material that absorbs the sunlight

spectrum[16].

  In this study, a new type of Sn-Ge-based perovskite was prepared. The preparation method was

based on the report by Zhao *et al.* who showed a highest efficiency of 8.12 % with

FA$_{0.75}$MA$_{0.25}$SnI$_3$[17]. The optical and electronic properties of the perovskite were determined

using UV-Vis measurement and photoacoustic spectroscopy. The data obtained from XRD and

XPS measurement was used to determine the chemical structure of the synthesized perovskite

material. At the same time the data obtained from the PAS measurement will afforded the

information on the disorder in the perovskite material. AFM measurement was performed to

observe the effect of Ge doping on the morphology of the FA$_{0.75}$MA$_{0.25}$SnI$_3$ and can be related to

the passivation of the surface defects. Finally, the J-V measurements were performed to elucidate

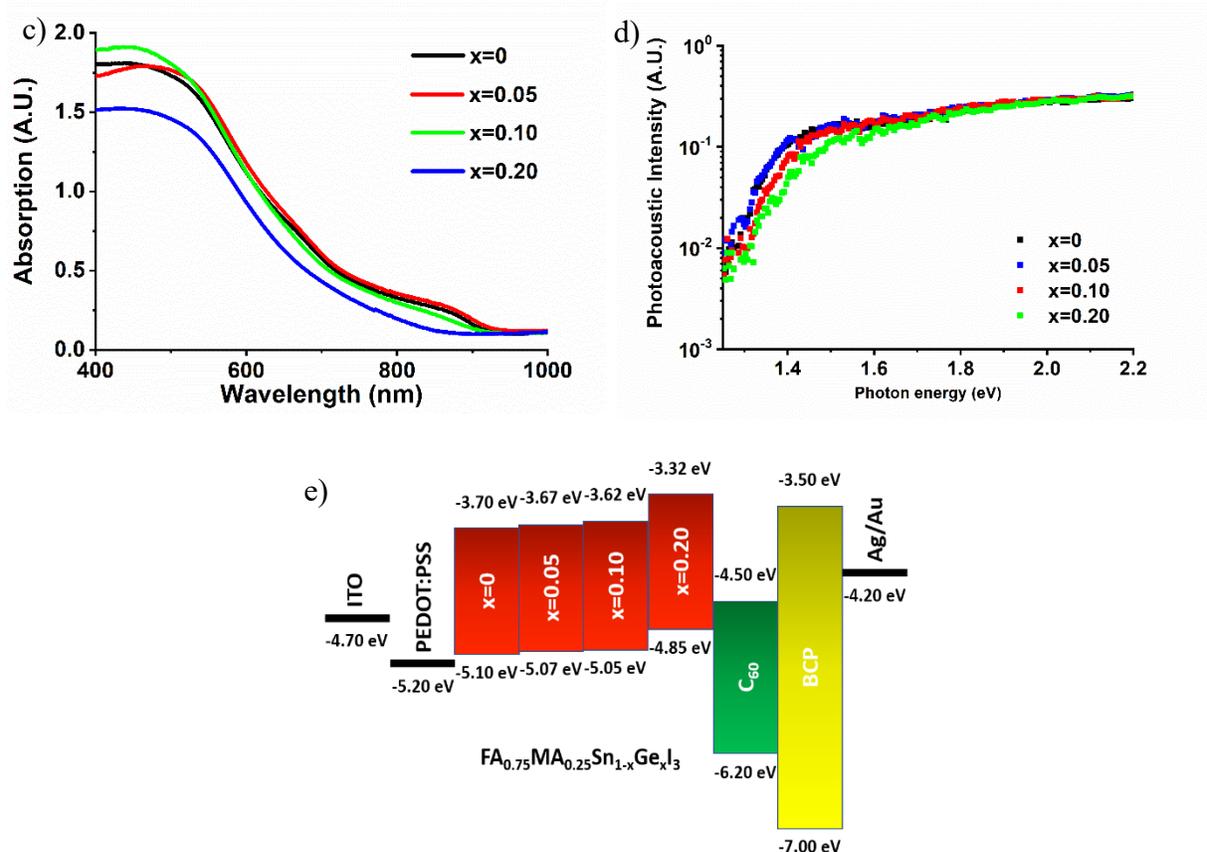the applicability of these materials in solar cell applications.
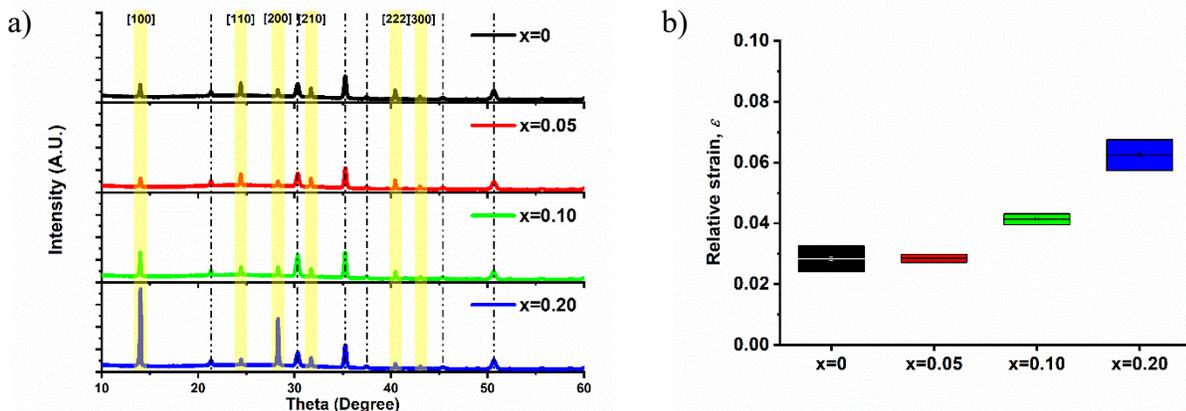
Figure 1. a) XRD patterns of $FA_{0.75}MA_{0.25}Sn_{1-x}Ge_xI_3$ thin films $\theta=10-80^o$, b) relative strain vs Ge concentration, c) UV-Vis absorption, d) photoacoustic signal intensity as a function of photon energy measured at room temperature and e) energy band diagram constructed from PAS and PYS measurement. The dotted lines correspond to signal from the PEDOT:PSS-coated ITO substrate.

XRD spectra were used to determine the structure of the synthesized perovskite materials. The XRD pattern for each material is given in Figure 1a. The XRD peaks of the perovskite were given around 14.5^o and 28° which corresponds with the hexagonal perovskite phase. Upon doping the $FA_{0.75}MA_{0.25}SnI_3$ perovskite material with Ge, no additional peak was observed showing that the perovskite structure has not been disrupted. The intensity of the peak at 14.5^o

increased significantly upon doping and the diffraction angles shifted towards larger angles. This could be attributed to the smaller ionic size of Ge filling the gap between large Sn ions and thus reducing the lattice parameters of $FA_{0.75}MA_{0.25}Sn_{1-x}Ge_xI_3$. The crystal size of the perovskite material is calculated using the Scherrer's equation[18,19]. Here the peak around 14° was used to calculate the crystal size. x=0.20 perovskite sample showed the largest crystal size of 78.8 nm, followed by $FA_{0.75}MA_{0.25}SnI_3$ (x=0) with 77.7 nm, 73.6 nm for x=0.10 sample, and the smallest crystal size was obtained with x=0.05 nm with 72.3 nm.

Further analysis of the XRD data gives the information on the relative strain as a function of Ge content (Figure 1b). The relative strain can be calculated using the Williamson-Hall plot using a linear fit. It is found that the relative strain is similar between x=0 and x=0.05, however higher concentration of doping resulted in higher lattice disorder. It has been reported that perovskite material with higher strain is prone to degradation due to ion migration and will affect the overall performance of solar cell[20]. The Williamson-Hall plot for each perovskite materials is given in Figure S1.

The optical properties of the synthesized perovskite materials were evaluated using UV-Vis measurement. As evidence from the spectra (Figure 1c), apart from x=0.05, increasing the Ge concentration shifted the absorption edges toward shorter wavelength. Interestingly, only x=0.05 sample showed higher absorption than pure Sn perovskite and this could result in higher J_{SC} for the solar cell. The E_g was 1.40 eV, 1.40 eV, 1.44 eV and 1.58 eV for x=0, x=0.05, x=0.10 and x=0.15, respectively.

To further evaluate the optical property of the perovskite material, photoacoustic spectroscopy (PAS) was performed. Figure 1d shows the plot of photoacoustic signal as a function of energy

where the E_g can be determined from shoulder of the curve. From the PAS measurement, the Urbach energy, E_u was also determined. It is an important parameter in crystalline material as it shows the order or disorder in a material. It relates to the presence of localized states originating from the top of the valence bands which extends into the band gap at low photon energy. The equation (Equation 1) for determining E_u is given by the optical absorption coefficient as follow

$$\alpha = \alpha_0 exp(\frac{hv-hv_0}{E_U})$$ (1)

where α_0 and hv_0 are fitting parameters which can be determined from temperature dependence measurement[21]. The E_u measured for $FA_{0.75}MA_{0.25}SnI_3$ was 37 meV while for x=0.05, it was 36 meV. However, increasing the Ge content increased the E_u which means that the crystal became more disordered. It is expected that when a disorder increased in a crystalline material, the defects or vacancies are created and thus the trap density increases. The steepness factor is inversely related to the E_u using the following equation (Equation 2)

$$E_U = \frac{k_B T}{\sigma(T)}$$ (2)

where k_B is the Boltzmann constant and $\sigma(T)$ is the steepness factor that depends on the temperature. It is mentioned that $\sigma(T)$ is inversely proportional to the binding energy between electrons/excitons and phonons. The steepness factors also showed the same trend as E_u where a decreasing trend was observed apart for x=0.05.

Table 1. Summary of electronic properties of the $FA_{0.75}MA_{0.25}Sn_{1-x}Ge_xI_3$ based on the PAS measurement.

Sample	Bandgap Energy (E_g)	Urbach Energy (E_U)	Steepness Factor
X=0	1.40 eV	37 meV	0.68
X=0.05	1.40 eV	36 meV	0.69
X=0.1	1.42 eV	38 meV	0.66
X=0.2	1.53 eV	63 meV	0.40

Photoelectron yield spectroscopy was used to measure the valence band of the perovskite materials (Figure S2). It is found that the valence band decreased with increasing Ge doping. Using the PYS data, the density of state (DOS) of the different perovskites can be determined (Figure S3). For x=0.05, DOS distribution is clearly lower than x=0 meaning that the number of available states for electron upon addition of Ge. It is expected that free charge carrier is less likely to be intercepted by these energy states. From the E_g values and valence band values, the conduction band values of the perovskites can be calculated. These are represented in the energy diagram in Figure 1e. It is apparent that doping with Ge both the valence and conduction band of $FA_{0.75}MA_{0.25}SnI_3$ were upshifted. This led to the mismatch between the work function of the ITO and the valence band of the perovskite materials. It seems counter intuitive that the large energy mismatch at the perovskite and PEDOT:PSS interface could allow electron transfer. The same phenomena have been observed by Zhao *et al*. in which the conduction band of their tin perovskite materials are higher than the work function of PEDOT:PSS but the perovskite

materials still show excellent photovoltaic performance[17]. They cited that the work function of

PEDOT:PSS has been upshifted up to -4.85 eV upon contact with the ammonium part of the

perovskite which reduces the surface of the PEDOT:PSS. This 'spike'-like energy level has been

discussed by Minemoto *et al*. providing a theoretical analysis of band offset in perovskite solar

cells either at electron transport material/perovskite or hole transport material/perovskite

interface[22]. It has been reported that an energy mismatch of up to 0.2 eV could still help to

improve the performance of the solar cell.
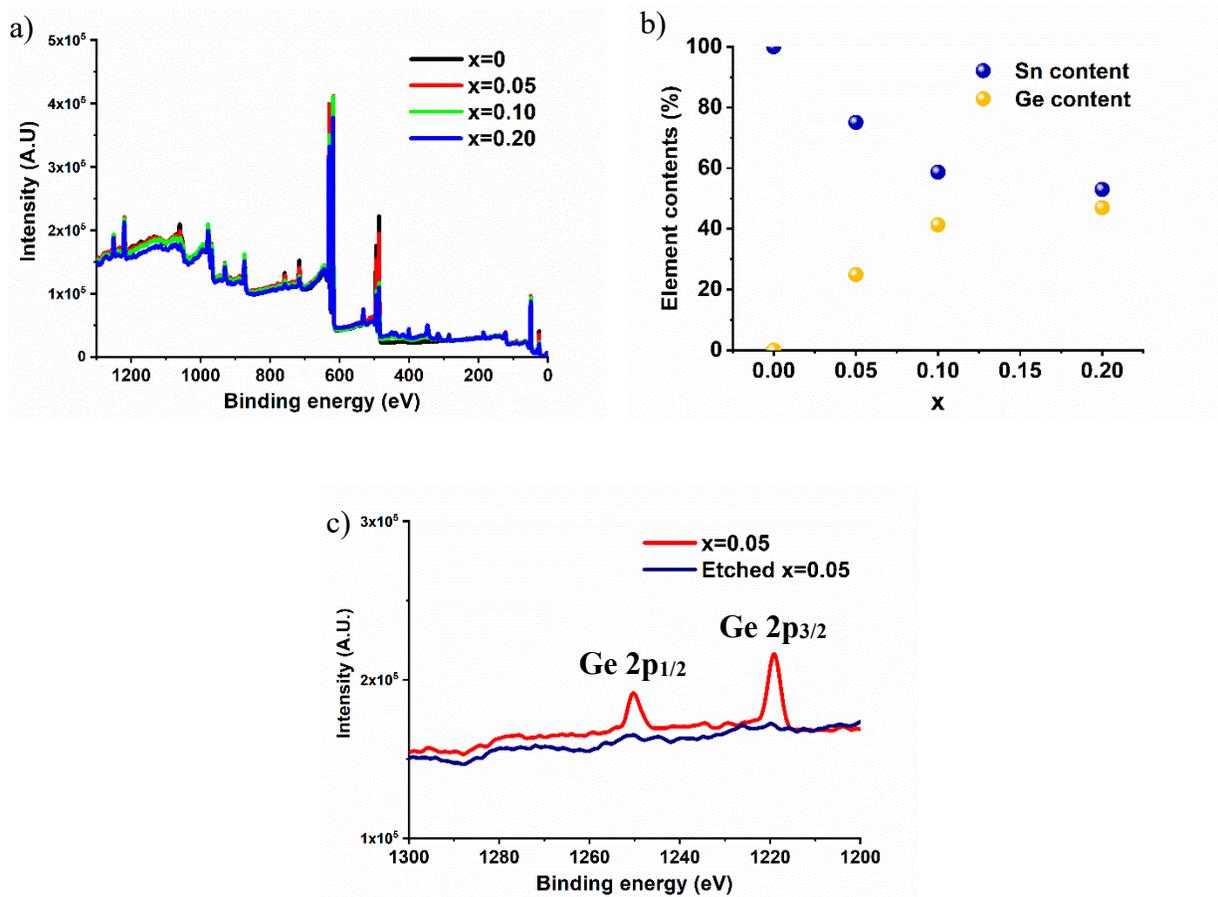

Figure 2. XPS profile for the $FA_{0.75}MA_{0.25}Sn_{1-x}Ge_xI_3$ materials. a) wide scan of the different

perovskites, b) the elemental composition of each sample, and c) comparison of Ge peaks before

and after Argon etching.

9

XPS spectra were recorded to further corroborate the formation of mixed Sn-Ge halide perovskite given in Figure 2a. For Sn, the Sn $3d_{5/2}$ and Sn $3d_{3/2}$ peaks are located at 486 eV and 494 eV, respectively (Figure S4a). For Ge, the $3d_{3/2}$ peak could be observed at 32 eV (Figure S4b). The trend observed here was that the Sn intensity decreased while the Ge intensity increased with higher Ge content which is as expected. The XPS spectra for the peak around 486 eV originating from Sn has been deconvoluted into 3 different peaks using Gaussian fitting corresponding to Sn^0, Sn^{2+} and Sn^{3+} as shown in Figure S5. After normalizing the intensity signal with respect to the value of x=0 sample, it is found that the intensity of Sn^{4+} decreases with Ge addition suggesting the passivation effect on Sn. Table S1 summarizes the difference in the intensity of Sn^{4+} upon doping with Ge. The elemental composition of the perovskite films was also obtained from XPS as shown in Figure 2b. As expected, the content of Ge increased from x=0 to x=0.2. However, even at lower Ge doping concentration of x=0.2, the content of Ge was almost half of the total metal content in the perovskite which is anomalous. It is known that the detection depth of XPS is limited to several nm. Thus, the elemental composition values obtained were not bulk properties but rather surface composition. To confirm this, Argon etching was performed on x=0.05 sample and through this process, a depth of several nm from the perovskite surface has been etched. The XPS spectra showing the difference before and after etching is given in Figure 2c. It is found that the content of Ge significantly decreased when going deeper into the perovskite. It can be concluded that most of the Ge atoms passivate the surface of the Sn perovskite due to their smaller ionic radii. This agrees with previous UV-Vis, PAS and XRD result which showed that at low concentration of Ge (x=0.05) no significant change in the E_g and the relative strain compared to pure $FA_{0.75}MA_{0.25}SnI_3$ due to surface passivation. However, it is

thought that upon higher concentration of Ge, the Ge atoms are distributed within the crystal lattice and hence significantly changed the E_g and the relative strain.
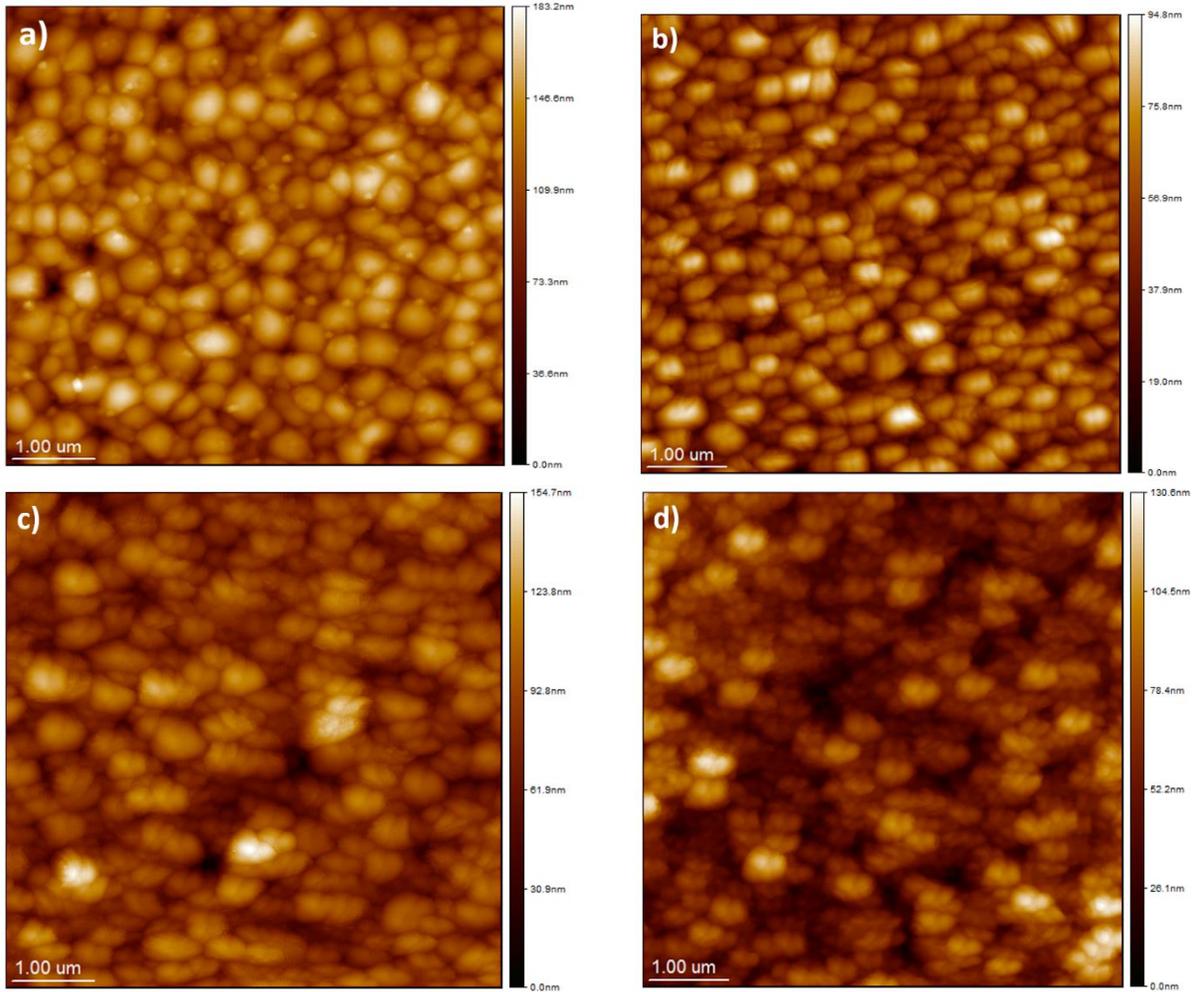

Figure 3. AFM images obtained from SPM for the $FA_{0.75}MA_{0.25}Sn_{1-x}Ge_xI_3$ perovskites. The surface roughness of the perovskite is given by the root-mean-square (R_q) value and the maximum thickness is given by the R_z value. a) x=0, b) x=0.05, c) x=0.10 and d) x=0.20.

The surface morphology was characterized by c-AFM using samples prepared on ITO substrates coated with PEDOT:PSS to replicate the solar cell structure (Figure 3). Doping $FA_{0.75}MA_{0.25}SnI_3$ with Ge clearly affected the grain size of the perovskite layer as seen from the

AFM images. Apart from x=0 perovskite, increasing the Ge concentration led to the increase in the grain size. This supports the grain size data calculated from the XRD patterns. In the case of $FA_{0.75}MA_{0.25}SnI_3$, the grains are bigger however the presence of smaller granules could be seen on the surface of the perovskite layer. The surface roughness has also been calculated from the c-AFM. Doping the $FA_{0.75}MA_{0.25}SnI_3$ with the Ge beneficially decreased the surface roughness from 21.4 nm for $FA_{0.75}MA_{0.25}SnI_3$, to 13.7 nm for x=0.05. The roughness for x=0.10 was 17.8 nm and x=0.20 was 19.9 nm. It is to be expected that since the ionic radius of Ge is smaller than that of Sn, and thus some of the Ge atoms are thought to have filled the defects/vacancies of $FA_{0.75}MA_{0.25}Sn_1I_3$ perovskites. This observation confirms the result obtained from XPS where Ge atoms were only found on the surface of the perovskite at low concentration of Ge. This means that the pinholes on $FA_{0.75}MA_{0.25}SnI_3$ have been successfully passivated by Ge and therefore reducing the surface roughness of $FA_{0.75}MA_{0.25}SnI_3$.
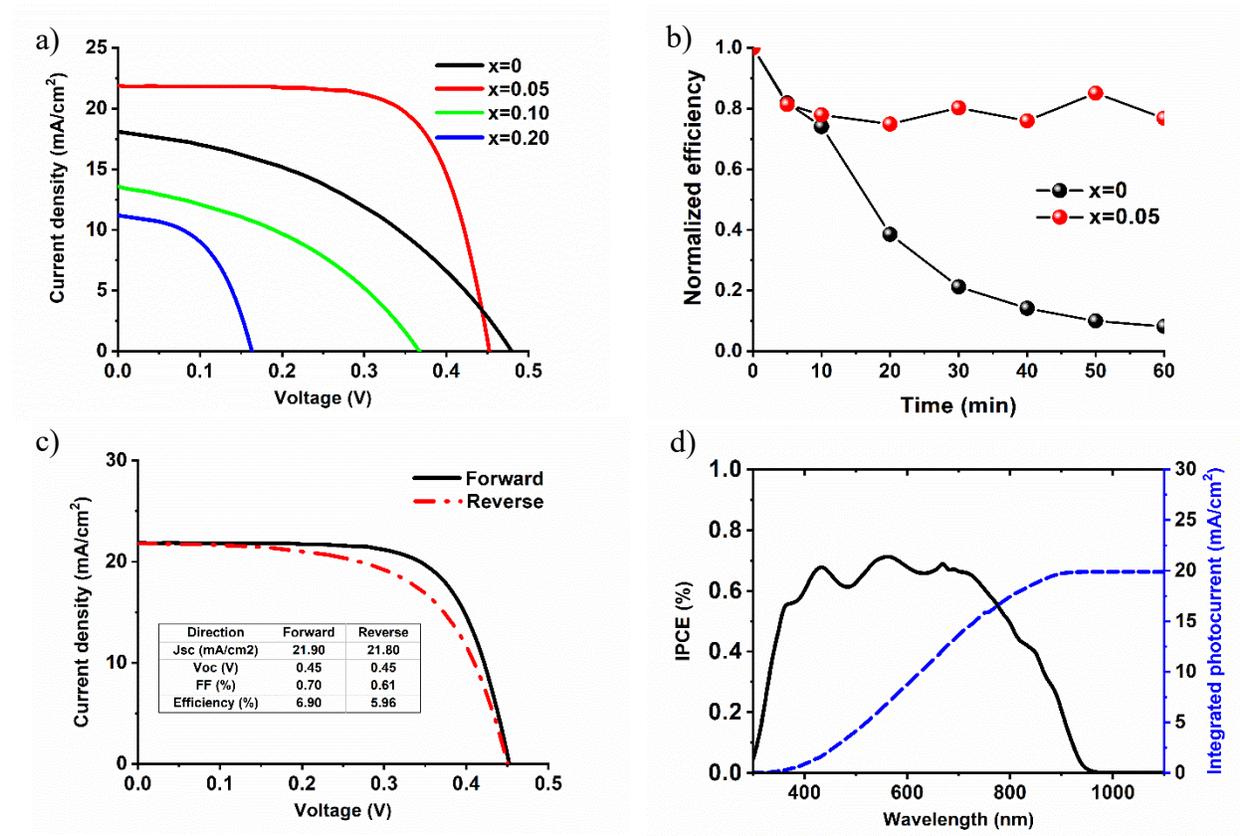
Figure 4. a) J-V curve of the best performing devices measured at room temperature under 1 sun illumination in air without encapsulation using a 0.10 cm^2 mask. b) Stability test of the best performing x=0 and x=0.05 solar cells. c) J-V curve of x=0.05 after 72 h, measured in air without encapsulation, and d) the corresponding EQE curve.

Figure 4a shows the J-V curves of the best performing devices for each type. Table 2 summaries the performance of each type of devices. For FA$_{0.75}$MA$_{0.25}$SnI$_3$ device, the average J$_{SC}$ was 17.61 mA/cm^2, V$_{OC}$ was 0.46 V, FF was 0.41 and PCE of 3.31 %. Upon doping with 5 wt% of Ge, the J$_{SC}$ increased up to 19.80 mA/cm^2, FF improved up to 0.55 with an overall efficiency of 4.48 %. However, the V$_{OC}$ decreased when compared with pure FA$_{0.75}$MA$_{0.25}$SnI$_3$ solar cell. Upon increasing the Ge content, all the photovoltaic parameters decreased significantly which resulted in an efficiency as low as 0.80 % for x=0.20 device. The high J$_{SC}$ in the case of x=0.05 can be attributed to the higher absorption as evidenced from the previous UV-Vis result. This means that the perovskite material has higher probability of exciting the excitons into free electrons and holes. The decreasing trend in the J$_{SC}$ for higher Ge content also follows the UV-Vis absorption trend.

Table 2. Summary of photovoltaic performance of the different FA$_{0.75}$MA$_{0.25}$Sn$_{1-x}$Ge$_x$I$_3$ solar cells based on 5 different devices for each type.

Device	V$_{OC}$	J$_{SC}$	FF	PCE	R$_s$	R$_{sh}$
	(V)	(mA/cm^2)	(%)	(%)	(Ω)	(Ω)
x=0	0.46	17.61	0.41	3.31	9.59	109.59

	± 0.03	± 0.6	± 0.01	± 0.27	± 0.59	± 16.04
x=0.05	0.42	19.50	0.55	4.48	4.01	227.96
	± 0.01	± 0.8	± 0.05	± 0.31	± 0.72	± 47.04
x=0.10	0.33	13.27	0.49	2.04	7.23	203.40
	± 0.05	± 4.1	± 0.07	± 0.44	± 2.98	± 131.11
x=0.20	0.15	11.84	0.46	0.80	3.75	100.33
	± 0.02	± 0.7	± 0.05	± 0.14	± 0.26	±49.70

The discussion on the effect of FF can be explained from the series resistance. It is a well-known phenomenon that the series resistance is affected by the resistance at the perovskite interface, electrode resistance and contact resistance[23]. As summarized in Table 2, the series resistance decreased upon doping with Ge, where R_S was determined from the slope of the J-V curve at the V_{OC}. Upon doping with x=0.05, the R_S decreases from 9.49 Ω to 4.01 Ω which can be explained from the better film morphology allowing for better contact with C_{60}, BCP and Ag. This can also explain the increase in the J_{SC} as the electrons are easily transported within the device. Increasing the doping further led to the increase of Ge thickness on the surface. This adversely affect the electron transport mechanism from the back electrode as the resistance also increase.

It has been reported that larger perovskite grain size gives better solar cell performance but this trend has not been observed in this work[24–26]. Despite showing higher crystal size, the performance of $FA_{0.75}MA_{0.25}SnI_3$ is lower than that of $FA_{0.75}MA_{0.25}Sn_{0.95}Ge_{0.05}I_3$. This indirectly

shows that apart from the grain size, other factors also affect the performance of the solar cell. In this case, Ge doping helped to reduce the trap density and defects in $FA_{0.75}MA_{0.25}SnI_3$ perovskite as observed from PAS measurement. The increased in the solar cell performance can also be explained from the formation of an efficient p-i-n hetero-junction structure upon doping with Ge. The high efficiency of hetero-junction structure perovskite solar cells has been discussed previously in detailed[27,28]. It also noted that in the case of Sn-based kesterite solar cell, doping with Ge improved the performance significantly citing the suppression of Sn oxidation and thus reducing the trap states which agrees with the finding in this work[29].

In Figure 4b, x=0.05 solar device showed superior stability in air where as high as 80 % of its original efficiency is still retained after 60 min compared to just 10 % of x=0 solar cell. As discussed previously, the surface passivation of Sn by Ge reduces the probability of the Sn^{2+} to be oxidized into Sn^{4+}. Interestingly, when the same device was measured after keeping in N_2 atmosphere for 72 h, the efficiency increased up to 6.90 % when measured in air (Figure 4c). It is noted that the device was kept in the dark in the glove box prior to measurement. Significant increment in the J_{SC} and FF led to the good performance of the solar cell. The calculated J_{sc} from the IPCE spectrum was 19.87 mA/cm^2 which agrees well with the value measured from the J-V curves (21.90 mA/cm^2) (Figure 4d). This phenomena has been observed by Roose *et al.* who reported that the coalescence of smaller grains into bigger grains which effectively reduces grain boundaries and at the same time suppresses the non-radiative recombination[30]. Another possible reason for this increase is due to the self-healing property of perovskite material in the dark as reported by Nie *et al.*[31].

In conclusion, a new type of perovskite having the structure of $FA_{0.75}MA_{0.25}Sn_{1-x}Ge_xI_3$ has been successfully prepared as confirmed from the XRD and XPS measurement. The electrical

and optical characteristics of the perovskite materials were evaluated using PA and UV-Vis measurement showed that the materials have E_g ranging from 1.40 to 1.53 eV which confirmed the hypothesis that these materials can be used for solar cell applications. The highest performance was obtained with Ge content of x = 0.05, showing J_{SC} 19.50 mA/cm^2, V_{OC} of 0.42 V, FF of 0.41 and efficiency of 4.48 %. The enhanced performance of this device when compared to that of $FA_{0.75}MA_{0.25}SnI_3$ (3.31 %) was attributed to the lower disorder/defects and hence the trap density in the perovskite material as observed from the PA measurement. The surface of $FA_{0.75}MA_{0.25}SnI_3$ has also been passivated by Ge at low concentration and thus it can be assumed the defects in $FA_{0.75}MA_{0.25}SnI_3$ which can cause recombination, has been effectively reduced. Additionally, the stability in air has been improved significantly with the Ge doping, retaining 80 % of its original performance remarkable stability enhancement, compared with 10 % efficiency retention for the non-doped perovskite solar cell. After 72 h in N_2 atmosphere, the same cell showed a high efficiency of 6.90 %. This work provides a platform for further research on lead-free Sn-Ge based perovskite solar cells.

AUTHOR INFORMATION

Corresponding Author

*E-mail: akmal-kamarudin@life.kyutech.ac.jp (M. A. K.); hayase@life.kyutech.ac.jp (S. H.)

Author Contributions

The manuscript was written through contributions of all authors. All authors have given approval to the final version of the manuscript.

Notes

The authors declare no competing financial interest.

ASSOCIATED CONTENT

Supporting Information.

The following files are available free of charge.

Materials, perovskite film fabrication, device fabrication, Williamson-Hall plot, PYS plot, DOS plot, XPS plot, photovoltaic parameters and summary of XPS intensity. (PDF)

REFERENCES

(1)   Kojima, A.; Teshima, K.; Shirai, Y.; Miyasaka, T. Organometal Halide Perovskites as Visible-Light Sensitizers for Photovoltaic Cells. *J. Am. Chem. Soc.* **2009**, *131*, 6050–6051.

(2)   Saliba, M.; Matsui, T.; Domanski, K.; Seo, J.-Y.; Ummadisingu, A.; Zakeeruddin, S. M.; Correa-Baena, J.-P.; Tress, W. R.; Abate, A.; Hagfeldt, A.; *et al*. Incorporation of Rubidium Cations into Perovskite Solar Cells Improves Photovoltaic Performance. *Science.* **2016**, *354*, 206–209.

(3)   Rühle, S. Tabulated Values of the Shockley-Queisser Limit for Single Junction Solar Cells. *Sol. Energy* **2016**, *130*, 139–147.

(4)   Unger, E. L.; Kegelmann, L.; Suchan, K.; Sörell, D.; Korte, L.; Albrecht, S. Roadmap and Roadblocks for the Band Gap Tunability of Metal Halide Perovskites. *J. Mater. Chem. A* **2017**, *5*, 11401–11409.

(5)   Dong, Q.; Fang, Y.; Shao, Y.; Mulligan, P.; Qiu, J.; Cao, L.; Huang, J. Electron-Hole Diffusion Lengths > 175 μm in Solution-Grown $CH_3NH_3PbI_3$ Single Crystals. *Science.* **2015**, *347*, 967–970.

(6)   Shi, D.; Adinolfi, V.; Comin, R.; Yuan, M.; Alarousu, E.; Buin, A.; Chen, Y.; Hoogland, S.; Rothenberger, A.; Katsiev, K.; *et al*. Low Trap-State Density and Long Carrier Diffusion in Organolead Trihalide Perovskite Single Crystals. *Science.* **2015**, *347*, 519–522.

(7)   Abate, A. Perovskite Solar Cells Go Lead Free. *Joule* **2017**, *4*, 1–6.

(8)   Giustino, F.; Snaith, H. J. Toward Lead-Free Perovskite Solar Cells. *ACS Energy Lett.* **2016**, *1*, 1233–1240.

(9)   Ogomi, Y.; Morita, A.; Tsukamoto, S.; Saitho, T.; Fujikawa, N.; Shen, Q.; Toyoda, T.; Yoshino, K.; Pandey, S. S.; Ma, T.; *et al*. $CH_3NH_3Sn_xPb_{(1-x)}I_3$ Perovskite Solar Cells Covering up to 1060 nm. *J. Phys. Chem. Lett.* **2014**, *5*, 1004–1011.

(10)   Shao, S.; Liu, J.; Portale, G.; Fang, H.-H.; Blake, G. R.; ten Brink, G. H.; Koster, L. J. A.; Loi, M. A. Highly Reproducible Sn-Based Hybrid Perovskite Solar Cells with 9% Efficiency. *Adv. Energy Mater.* **2017**, *8*, 1-10.

(11)   Noel, N. K.; Stranks, S. D.; Abate, A.; Wehrenfennig, C.; Guarnera, S.; Haghighirad, A.-A.; Sadhanala, A.; Eperon, G. E.; Pathak, S. K.; Johnston, M. B.; *et al*. Lead-Free Organic–inorganic Tin Halide Perovskites for Photovoltaic Applications. *Energy Environ. Sci.* **2014**, *7*, 3061–3068.

(12)   Liao, Y.; Liu, H.; Zhou, W.; Yang, D.; Shang, Y.; Shi, Z.; Li, B.; Jiang, X.; Zhang, L.; Quan, L. N.; *et al*. Highly Oriented Low-Dimensional Tin Halide Perovskites with Enhanced Stability and Photovoltaic Performance. *J. Am. Chem. Soc.* **2017**, *139*, 6693–6699.

(13)   Rajendra Kumar, G.; Kim, H. J.; Karupannan, S.; Prabakar, K. Interplay between Iodide and Tin Vacancies in CsSnI$_3$ Perovskite Solar Cells. *J. Phys. Chem. C.* **2017**, *121*, 16447–16453.

(14)   Stoumpos, C. C.; Frazer, L.; Clark, D. J.; Kim, Y. S.; Rhim, S. H.; Freeman, A. J.; Ketterson, J. B.; Jang, J. I.; Kanatzidis, M. G. Hybrid Germanium Iodide Perovskite Semiconductors: Active Lone Pairs, Structural Distortions, Direct and Indirect Energy Gaps, and Strong Nonlinear Optical Properties. *J. Am. Chem. Soc.* **2015**, *137*, 6804–6819.

(15)   Krishnamoorthy, T.; Ding, H.; Yan, C.; Leong, W. L.; Baikie, T.; Zhang, Z.; Li, S.; Asta, M.; Mathews, N.; Mhaisalkar, S. G.; *et al*. Lead-Free Germanium Iodide Perovskite Materials for Photovoltaic Application. *J. Mater. Chem. A.* **2015**, *3*, 23829–23832.

(16)   Ju, M. G.; Dai, J.; Ma, L.; Zeng, X. C. Lead-Free Mixed Tin and Germanium Perovskites for Photovoltaic Application. *J. Am. Chem. Soc.* **2017**, *139*, 8038–8043.

(17)   Zhao, Z.; Gu, F.; Li, Y.; Sun, W.; Ye, S.; Rao, H.; Liu, Z.; Bian, Z.; Huang, C. Mixed-Organic-Cation Tin Iodide for Lead-Free Perovskite Solar Cells with an Efficiency of 8.12%. *Adv. Sci.* **2017**, *4*, 1–7.

(18)   Heo, J. H.; Lee, M. H.; Jang, M. H.; Im, S. H. Highly Efficient $CH_3NH_3PbI_{3-x}Cl_x$ Mixed Halide Perovskite Solar Cells Prepared by Re-Dissolution and Crystal Grain Growth via Spray Coating. *J. Mater. Chem. A.* **2016**, *4*, 17636–17642.

(19)   Patterson, A. L. The Scherrer Formula for X-Ray Particle Size Determination. *Phys. Rev.* **1939**, *56*, 978–982.

(20)   Zhao, J.; Deng, Y.; Wei, H.; Zheng, X.; Yu, Z.; Shao, Y.; Shield, J. E.; Huang, J. Strained Hybrid Perovskite Thin Films and Their Impact on the Intrinsic Stability of Perovskite Solar Cells. *Sci. Adv.* **2017**, *3*, 1–8.

(21)   Urbach, F. The Long-Wavelength Edge of Photographic Sensitivity and of the Electronic Absorption of Solids. *Phys. Rev.* **1953**, *92*, 1324.

(22)   Minemoto, T.; Murata, M. Theoretical Analysis on Effect of Band Offsets in Perovskite Solar Cells. *Sol. Energy Mater. Sol. Cells* **2015**, *133*, 8–14.

(23)   Li, Y.; Ding, B.; Chu, Q. Q.; Yang, G. J.; Wang, M.; Li, C. X.; Li, C. J. Ultra-High Open-Circuit Voltage of Perovskite Solar Cells Induced by Nucleation Thermodynamics on Rough Substrates. *Sci. Rep.* **2017**, *7*, 1–10.

(24)   Ren, X.; Yang, Z.; Yang, D.; Zhang, X.; Cui, D.; Liu, Y.; Wei, Q.; Fan, H.; Liu, S. Modulating Crystal Grain Size and Optoelectronic Properties of Perovskite Films for Solar Cells by Reaction Temperature. *Nanoscale* **2016**, *8*, 3816–3822.

(25)   Chen, J.; Shi, T.; Li, X.; Zhou, B.; Cao, H.; Wang, Y. Origin of the High Performance of Perovskite Solar Cells with Large Grains. *Appl. Phys. Lett.* **2016**, *108*, 1–4.

(26) Chiang, C. H.; Wu, C. G. Film Grain-Size Related Long-Term Stability of Inverted

Perovskite Solar Cells. *ChemSusChem* **2016**, *9*, 2666–2672.

(27) Jeng, J. Y.; Chiang, Y. F.; Lee, M. H.; Peng, S. R.; Guo, T. F.; Chen, P.; Wen, T. C.

$CH_3NH_3PbI_3$ Perovskite/fullerene Planar-Heterojunction Hybrid Solar Cells. *Adv. Mater.*

2013, *25*, 3727–3732.

(28) Docampo, P.; Ball, J. M.; Darwich, M.; Eperon, G. E.; Snaith, H. J. Efficient Organometal

Trihalide Perovskite Planar-Heterojunction Solar Cells on Flexible Polymer Substrates.

Nat. Commun. **2013**, *4*, 1-6.

(29) Giraldo, S.; Neuschitzer, M.; Thersleff, T.; Lõpez-Marino, S.; Sánchez, Y.; Xie, H.;

Colina, M.; Placidi, M.; Pistor, P.; Izquierdo-Roca, V.; *et al*. Large Efficiency

Improvement in $Cu_2ZnSnSe_4$ Solar Cells by Introducing a Superficial Ge Nanolayer. *Adv.*

Energy Mater. **2015**, *5*, 1–6.

(30) Roose, B.; Ummadisingu, A.; Correa-Baena, J. P.; Saliba, M.; Hagfeldt, A.; Graetzel, M.;

Steiner, U.; Abate, A. Spontaneous Crystal Coalescence Enables Highly Efficient

Perovskite Solar Cells. *Nano Energy* **2017**, *39*, 24–29.

(31) Nie, W.; Blancon, J.-C.; Neukirch, A. J.; Appavoo, K.; Tsai, H.; Chhowalla, M.; Alam, M.

A.; Sfeir, M. Y.; Katan, C.; Even, J.; *et al*. Light-Activated Photocurrent Degradation and

Self-Healing in Perovskite Solar Cells. *Nat. Commun.* **2016**, *7*, 1–9.